ACS APPLIED MATERIALS & INTERFACES

Research Article

www.acsami.org

Activating Aluminum Reactivity with Fluoropolymer Coatings for Improved Energetic Composite Combustion

Jena McCollum,[†] Michelle L. Pantoya,*[,†] and Scott T. Iacono[‡]

[†]Department of Mechanical Engineering, Texas Tech University, Lubbock, Texas 79409, United States

[‡]Department of Chemistry and Chemistry Research Center, United States Air Force Academy, 2355 Fairchild Drive, Suite 2N225, Colorado Springs, Colorado 80840, United States

ABSTRACT: Aluminum (Al) particles are passivated by an aluminum oxide (Al_2O_3) shell. Energetic blends of nanometer-sized Al particles with liquid perfluorocarbon-based oxidizers such as perfluoropolyethers (PFPE) excite surface exothermic reaction between fluorine and the Al_2O_3 shell. The surface reaction promotes Al particle reactivity. Many Al-fueled composites use solid oxidizers that induce no Al_2O_3 surface exothermicity, such as molybdenum trioxide (MoO_3) or copper oxide (CuO). This study investigates a perfluorinated polymer additive, PFPE, incorporated to activate Al reactivity in Al−CuO and Al−MoO_3. Flame speeds, differential scanning calorimetry (DSC), and quadrupole mass spectrometry (QMS) were performed for varying percentages of PFPE blended with Al/MoO_3 or Al/CuO to examine reaction kinetics and combustion performance. X-ray photoelectron spectroscopy (XPS) was performed to identify product species. Results show that the performance of the thermite−PFPE blends is highly dependent on the bond dissociation energy of the metal oxide. Fluorine−Al-based surface reaction with MoO_3 produces an increase in reactivity, whereas the blends with CuO show a decline when the PFPE concentration is increased. These results provide new evidence that optimizing Al combustion can be achieved through activating exothermic Al surface reactions.

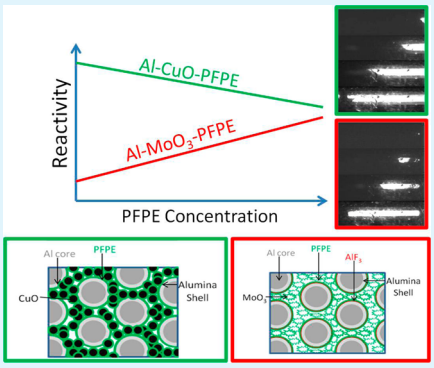

KEYWORDS: *aluminum powder, fluorine, combustion, aluminum fluoride, oligomers, energetic materials, exothermic surface chemistry, preignition reaction*

INTRODUCTION

A thermite is defined as an energetic system consisting of a metal fuel (i.e., aluminum (Al)) and a metal oxide (i.e., copper oxide (CuO) or molybdenum trioxide (MoO_3)).[1−6] These systems are widely studied due to their high energy densities and heats of combustion.[1−6] As energy-generating materials, thermite reactions have applications ranging from material synthesis[7−9] and alloying[10,11] to welding and joining.[12,13] Munir et al. presented a thorough review on thermite applications,[1] Fischer and Grublic tabulated thermochemical properties for hundreds of thermite reactions,[14] and Koch presented the chemistry and application of fluorocarbon-based energetics.[15] All of these reference materials provide a fundamental understanding of thermite reactivity and applications.

For Al-based thermites, when fluorine replaces oxygen as the oxidizing agent, aluminum fluoride (AlF_3) is formed instead of aluminum oxide (Al_2O_3). Both AlF_3 and Al_2O_3 are comparably thermodynamically stable with heats of formation of 1510 and 1676 kJ/mol, respectively.[15] However, AlF_3 formation is preferred to Al_2O_3 because Al−F (664 ± 6 kJ/mol)[16] bond formation is stronger than the Al−O bond (512 ± 4 kJ/mol).[16] In fact, F has been shown to react with the alumina passivation shell surrounding an Al particle.[17,18] The exothermic surface reaction precedes the main Al oxidation reaction and has been coined a pre-ignition reaction (PIR).[17] Kappagantula et al. showed that the PIR can be used to enhance Al reactivity.[19]

Typically, Al−fluoropolymer blends are prepared with a solid fluorinated oxidizer such as polytetrafluoroethylene (PTFE).[17,18,20−22] Solid PTFE introduces a limit to the fuel−oxidizer contact surface area, which is thought to limit the combustion performance.[19] In an attempt to resolve the limitation caused by fuel−oxidizer contact surface area, Kappagantula et al.[19] investigated the combustion of Al particles with surface-functionalized self-assembled monolayers (SAM). The SAM consisted of perfluorotetradecanoic (PFTD) acid bonded to the Al particle's native oxide shell (Al_2O_3). Surface functionalized Al−PTFD was successful in increasing the reactivity of Al particles combined with MoO_3 and produced an 86% increase in flame speed compared to Al−MoO_3 alone.[19] The enhancement in reactivity was attributed to the PIR resulting from the fluorine functionalization.

Another method for coating the Al surface that can be easily implemented is to introduce a liquid perfluorinated oligomer that phyisoabsorbs onto the Al particle surface.[23] Similar to results shown by Kappagantula et al.,[19] the liquid fluoro-oligomer may readily activate the PIR and promote greater overall Al reactivity. The liquid fluoro-oligomer used in this study is a class of viscous fluorinated oligomers called

Received: June 15, 2015
Accepted: August 6, 2015
Published: August 12, 2015

DOI: 10.1021/acsami.5b05238
ACS Appl. Mater. Interfaces 2015, 7, 18742−18749

perfluoropolyethers (PFPEs). Miller et al.[23] used a PFPE protective coating on nanoscale Al because of its thermal stability at low temperatures (up to 316 °C in an oxygen-rich environment) and potential to produce exothermic activity beyond 316 °C.[23] When coated with PFPE, the Al particles were able to suspend in a structural epoxy-based matrix. Miller used differential scanning calorimetry (DSC) to study the exothermic behavior for Al−perfluoropolyether (PFPE) blends of various weight percents. The DSC revealed two exothermic peaks, one of which occurred at the PFPE decomposition temperature of 316 °C (i.e., the PIR). The 30% Al/70% PFPE blend produced the highest heat of combustion. This formulation corresponds to an equivalence ratio (ER) of 1.2 (i.e., slightly fuel rich).

Previously, fundamental combustion analysis was performed for Al−PFPE blends.[23−25] The composites were characterized by a suite of thermal techniques including DSC, open burn rate, and heat of combustion measurements. The results showed that there is a balance to optimizing Al particle reactivity between activating Al particles with exothermic surface reactions and an excess of unreacted alumina that acts as a thermal heat sink during energy generation. These studies were focused on developing nanothermite fabrics that used Al−PFPE blends as an additive to provide the energetic component to the structural material. In these applications, flame speeds were on the order of millimeters per second. These results introduced a new and simplified synthesis approach for activating Al particle reactivity using a liquid fluoro-oligomer and the alumina shell as a catalyst to promote exothermic surface reactions.

The objective of this study is to use PFPE as an additive in different thermite systems (Al−MoO_3 and Al−CuO) to determine how the perfluorinated oligomer affects reaction kinetics and overall reactivity. The metal oxides MoO_3 and CuO were selected on the basis of their extensive use in research[6,26−29] and their differing dissociation properties. Specifically, the dissociation energy for the Mo−O bond is 607 ± 34 kJ/mol,[30] but the Cu−O bond energy is only 343 ± 63 kJ/mol.[30] Using a PFPE coating in these thermite systems could extend their shelf life by limiting particle surface exposure to oxygen-rich environments while exploiting exothermic surface reaction with the alumina shell that may contribute to enhancing overall reactivity.

EXPERIMENTAL SECTION

Materials. Aluminum powder (100 nm average particle diameter) with 3 nm Al_2O_3 particle shell thickness was procured from U.S. Nanomaterials (Houston, TX, USA). The PFPE (Fomblin Y LVAC 25/6, average molecular weight of 3300 g mol^{-1}) and the CuO (50 nm average particle diameter (spherical)) powder were supplied by Sigma-Aldrich (St. Louis, MO, USA). The MoO_3 (44 nm average particle diameter (flake structures)) was received from Nanostructured & Amorphous Materials, Inc. (Houston, TX, USA).

The composites were prepared to an equivalence ratio of 1.2 (i.e., slightly fuel rich). Equivalence ratio is shown in eq 1, where M is the mass, the fuel is Al, and the oxidizer is PFPE/CuO or PFPE/MoO_3.

$$\phi = \frac{\left[\frac{M_{\text{fuel}}}{M_{\text{oxidizer}}}\right]_{\text{actual}}}{\left[\frac{M_{\text{fuel}}}{M_{\text{oxidizer}}}\right]_{\text{stoichiometric}}} \quad (1)$$

The equivalence ratio was maintained constant for all samples by performing a molar balance using eqs 2 and 3, where a, b, c, d, and e are coefficients used to balance each reaction and P represents other products of the reaction (i.e., Al_4C_3 and Mo for eq 2 and Al_4C_3 and Cu for eq 3).

$$aCF_3O - [-CF(CF_3)CF_2O -]_x(-CF_2O -)_yCF_3 + bAl + cMoO_3 \rightarrow dAl_2O_3 + eAlF_3 + P \quad (2)$$

$$aCF_3O - [-CF(CF_3)CF_2O -]_x(-CF_2O -)_yCF_3 + bAl + cCuO \rightarrow dAl_2O_3 + eAlF_3 + P \quad (3)$$

The PFPE concentration was calculated such that PFPE accounts for 0, 5, 10, and 20 wt % of the reaction. The weight percent of each component is shown in Table 1.

Table 1. Weight Percent of All Components in Each Sample

	Al	oxidizer	PFPE
Al−CuO		CuO	
0	24 ± 0.1	76 ± 0.1	0
5	23 ± 0.1	73 ± 0.1	5 ± 0.1
10	22 ± 0.1	69 ± 0.1	9 ± 0.1
20	21 ± 0.1	63 ± 0.1	16 ± 0.1
Al−MoO_3		MoO_3	
0	34 ± 0.1	66 ± 0.1	0
5	34 ± 0.1	62 ± 0.1	4 ± 0.1
10	33 ± 0.1	59 ± 0.1	8 ± 0.1
20	32 ± 0.1	51 ± 0.1	17 ± 0.1

The PFPE, Al, and CuO or MoO_3 were weighed and suspended in 60 mL of Perfluorosolv PFS-2 from SPI Supplies (West Chester, PA, USA). The fluorinated solvent (PFS-2) was included to improve PFPE dispersion. The fluorine in the solvent disperses PFPE and suspends the Al/CuO or Al/MoO_3 particles to promote better coating. It is noted that non-fluorine-based solvents such as acetone and hexane did not disperse PFPE well enough to create a homogeneous mixture and were not adequate solvents for this synthesis application. The solution was then mixed using a planetary mixer at 1500 rpm for 2 min and poured into a Pyrex dish. The Perfluorosolv evaporated in a fume hood until the remaining mass was only that of Al/CuO/PFPE or Al/MoO_3/PFPE (e.g., about 24 h). Because of the high surface area of the Al/CuO and Al/MoO_3 and low concentration of PFPE, the samples were reclaimed as loose powders. Extensive microscopy analyses were performed by Iacono et al.[24] to establish Al particle coating by PFPE. The solid particle loadings in this study are similar to that produced in ref 24 such that similar microscopy is assumed.

Flame Speed Measurements. The powder was loaded into 3 mm inner diameter, 8 mm outer diameter, 10 cm long quartz tubes containing 300 mg of powder each (Figure 1a). The tubes are filled to a constant bulk density corresponding to 10% of the theoretical maximum density (TMD). Both ends of the tube were sealed with one side securing a length of nickel−chromium wire, bent into a "V" shape, and used for ignition by subjecting the wire to a voltage. Flame propagation was observed through a viewing window in the chamber. The reaction was recorded with a Phantom v7 (Vision Research, Wayne, NJ, USA) high-speed camera at a rate of 29 000 frames per second and aligned perpendicular to the direction of flame propagation. The flame speed was determined by tracking the flame front through a referenced time and distance using the Vision Research software. The resolution of the flame speed for this diagnostic is 0.1 m/s. Flame speeds were collected from five sets of experiments to establish repeatability. Repeatability of the measurements confirms good homogeneity in mixing and negligible density gradients with steady state propagation.

Thermal Equilibrium Analysis. Simultaneous thermal analysis (STA) was performed using a Netzsch Jupiter STA 449 differential scanning calorimeter and thermogravimetric analyzer (DSC/TGA). The samples were heated at 5 °C/min from room temperature to 1000 °C. Approximately 10 mg samples were loaded into crucibles and

DOI: 10.1021/acsami.5b05238
ACS Appl. Mater. Interfaces 2015, 7, 18742−18749

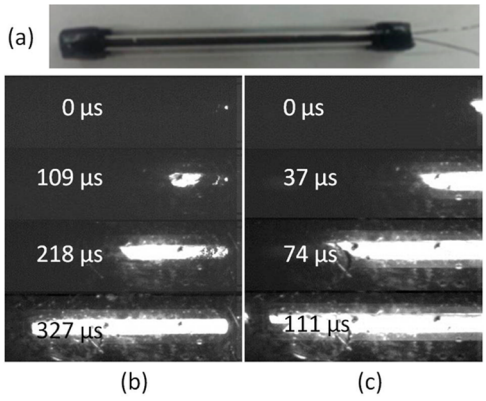

Figure 1. Representative time-stamped still frame images of powder-filled quartz tube and flame propagation: (a) sample-filled quartz tube prior to ignition (bulk density is 10% theoretical maximum density) and mixture is (b) Al/MoO_3 or (c) Al/CuO.

placed into the STA. Sintering can occur during heating and melting, ultimately affecting heat transfer in the STA measuring head. To ensure consistency and repeatability and to minimize artifact alterations of results, five experiments were performed for each sample. Temperature calibrations for the instrument were performed using melting of a set of metal standards resulting in a temperature accuracy of ±1 °C.

Gas species were identified using a Netzsch Aeolos 403 C quadrupole mass spectrometer to probe for the onset and relative magnitude of gaseous fluorine during the STA thermal cycle. Each spectrum is loaded into Netzsch Proteus software to identify species and magnitude as a function of temperature. Probes were programmed to collect the following species (with probed molecular mass in parentheses): HF (19), H_2O (18), CO_2 (44), CF_2 (50), and CF_3 (69). Because H_2O, CO_2, CF_2, and CF_3 made up only 2% of the total gas signal, the focus will be on HF.

X-ray Photoelectron Spectroscopy (XPS). XPS was performed on the reaction products using a PHI 5000 Versa Probe with an Al Kα source. Samples were loaded in a vacuum chamber, which was held to 1×10^{-6} Torr during measurement. Peaks were referenced to a C 1s value of 284.8 eV. For the MoO_3-based thermite (MBT) samples, the survey spectra identified Al, Mo, O, F, and C. The CuO-based thermite (CBT) survey spectra identified Al, Cu, O, F, C, and Na. Due to the presence of Na, analysis was performed on the O 2s peak because the O 1s peak was impeded by a Na 1s peak.

RESULTS AND DISCUSSION

Flame speed results for the two thermite systems as a function of PFPE concentration are shown in Figure 2 (and illustrated in Figure 1b,c). Overall, all of these mixtures produce flame speeds on the order of ~100 m/s and thus may be suitable for propellant applications. However, previous research with Al–PFPE blends was tailored toward high-temperature burning applications that were not necessarily suitable as propellants and produced flame speeds on the order of only 1 mm/s.[23−25] Specifically, when Al particles are incorporated into epoxy blends for structural energetic materials, PFPE is necessary to prevent Al from settling upon curing. The results shown here have the potential to transform pyrolant burning of structural energetics by adding metallic oxide particles (e.g., CuO or MoO_3) in addition to Al–PFPE into the epoxy matrix.

Figure 2 shows that the addition of PFPE yields different results with regard to oxidizing agent. The MoO_3-based thermites (MBT) benefit from the addition of PFPE, showing a continuous increase in flame speed (37% with the highest PFPE concentration). The CuO-based thermites (CBT) show the opposite trend: flame speed decreases as the PFPE concentration increases, with a decrease of 7% for the highest PFPE concentration.

The key question in this analysis is how fluorine from PFPE participates in the reactions. When combined with Al, the resulting product will be Al_2O_3 if Al reacts with oxygen reducing agents (i.e., CuO or MoO_3) and AlF_3 if Al reacts with the PFPE. The equivalence ratio (Φ = 1.2) was maintained constant for all samples such that the oxygen and fluorine have equal availability to react with Al.

Figure 3 shows the thermal analysis for 100 nm Al and PFPE alone. The results for onset and heat of combustion of each peak are shown in Table 2. Figure 4 shows heat flow curves from thermal analysis for CBT and MBT from 280 to 380 °C. The magnitude of the CBT pre-ignition reaction (PIR) builds with PFPE loading (Figure 4a), but is significantly less than that

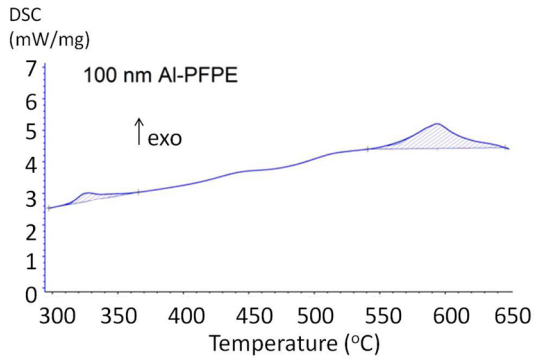

Figure 3. Oxidation reaction of 100 nm Al and PFPE heated from 35 to 1000 °C at 5 °C/min.

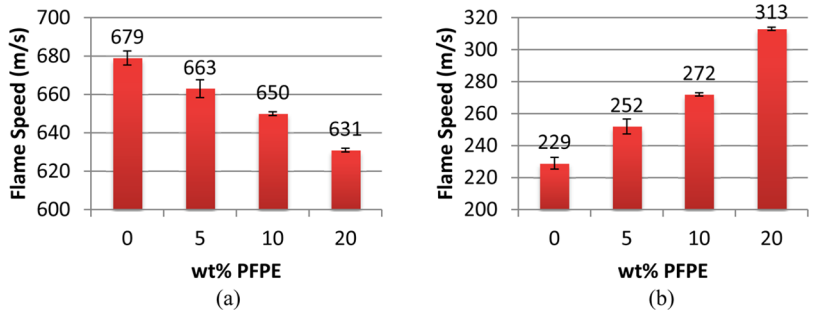

Figure 2. Flame propagation velocity for Al with (a) CuO and (b) MoO_3 with various percentages of PFPE. Equivalence ratio remains constant for all mixtures.

DOI: 10.1021/acsami.5b05238
ACS Appl. Mater. Interfaces 2015, 7, 18742−18749

Table 2. Results for the DSC Analysis of Al−CuO and Al−MoO_3 with *x*% of PFPE

sample	PIR onset temperature (°C)	PIR ΔH_c (J/g)	thermite reaction onset temperature (°C)	thermite reaction ΔH_c (J/g)
Al + PFPE	315 ± 0.1	19.8 ± 1.0	561 ± 0.1	133 ± 2
Al + CuO + 0% PFPE			517 ± 0.1	763 ± 2
Al + CuO + 5% PFPE	298 ± 0.1	19.56 ± 1.0	569 ± 0.1	1658 ± 3
Al + CuO + 10% PFPE	299 ± 0.1	29.70 ± 1.5	581 ± 0.1	1305 ± 2
Al + CuO + 20% PFPE	303 ± 0.1	51.37 ± 1.5	583 ± 0.1	843 ± 2
Al + MoO_3 + 0% PFPE			508 ± 0.1	2078 ± 3
Al + MoO_3 + 5% PFPE	298 ± 0.1	21.79 ± 1.0	534 ± 0.1	1370 ± 3
Al + MoO_3 + 10% PFPE	301 ± 0.1	35.17 ± 1.5	541 ± 0.1	1672 ± 3
Al + MoO_3 + 20% PFPE	305 ± 0.1	103.1 ± 2.0	566 ± 0.1	1889 ± 3

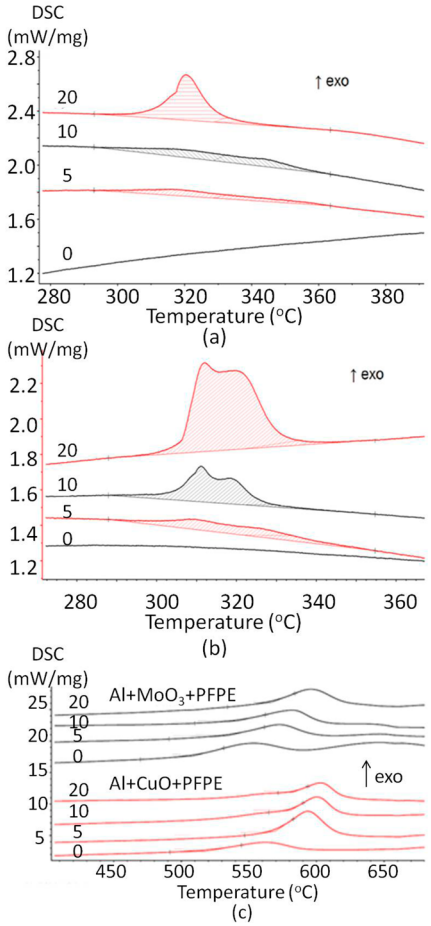

Figure 4. Pre-ignition reaction exotherm for aluminum with (a) CuO (PIR region) or (b) MoO_3 (PIR region) and (c) MBT and CBT (400−700 °C region). Samples were heated at 5 °C/min from 35 to 1000 °C in a 20% O_2/80% Ar by volume environment.

of the MBT (Figure 4b). Also, the onset of the PIR is around 307 °C for both CBT and MBT. Table 2 shows the magnitudes of the PIR for each sample. This low-temperature exotherm has been identified by others as the PIR and is associated with AlF_3 formation reactions.[17−19,23,31]

The thermal analysis from 400 to 700 °C for all samples is shown in Figure 4c, and the results are summarized in Table 2. The onset temperature of the main reaction increases with both CBT and MBT as PFPE concentration increases. Also, the magnitude of the main reaction produces a continuously increasing heat of combustion (calculated as the area under the curve) with increasing PFPE for both metal oxide blends. As the amount of PFPE increases, both onset temperatures surpass the onset temperature for Al oxidation at 565 °C when heated with PFPE alone (Figure 3). It is noted that PIRs are not shown in Figure 4c because the difference in magnitude between the PIR and main reaction is too large to distinguish the smaller PIR peaks.

From Figures 2−4, an increase in flame speed was observed with increase in PFPE for MBT, and also MBT shows that the PIR grows in exothermicity as PFPE concentration increases (Figure 4b). These results suggest that fluorine contribution to the reaction increases as the PFPE concentration increases, and this growing PIR may correlate to an increase in flame speed with PFPE concentration. In contrast, Figures 2−4 show CBT exhibits a decrease in flame speed with PFPE concentration and the PIR is significantly smaller than that of the MBT samples (see Table 2). Without significant contribution from the early-stage PIR (Table 2), chemical energy liberated from the reaction is delayed to higher onset temperature, thereby limiting energy propagation and reducing flame speed.

The opposite trends in flame speed shown in Figure 2 may depend on the bond dissociation energy (BDE) of the different metal oxidizers. The energy to break the Cu−O bond is only 343 ± 63 kJ/mol, but for the Mo−O bond it is 607 ± 34 kJ/mol.[30] The fluorine received from the PFPE is bonded to carbon, and the BDE of that bond is 536 ± 21 kJ/mol,[30] that of the carbon−carbon bond is 607 ± 21 kJ/mol,[30] and that of the carbon−oxygen bond is 1076.5 ± 4 kJ/mol.[30] Crouse et al. suggested that a possible mechanism for Al_2O_3-catalyzed reaction with PTFE involves the chemisorption of a CF_2 radical.[32] The energy needed to dislodge an oxygen atom from CuO to react with Al is significantly lower than the energy needed to extract fluorine alone from PFPE or to extract the CF_2 radical by breaking the C−C bond in the PFPE. For this reason, the PFPE reaction with Al may be overshadowed in the CBT because O is more readily available to oxidize Al (i.e., 343 vs 607 m/s). However, when the blends are made with an oxidizer with a higher BDE (i.e., MoO_3), the PFPE has a greater chance to participate in the reaction because the energy needed to extract fluorine (or CF_2 radical) and oxygen atoms from their respective reducing agents are similar. This can be confirmed by analyzing the products of the different reactions to identify the presence of AlF_3 in the different samples.

Hydrogen fluoride (HF) gas generation was monitored during thermal analysis and is shown as a function of temperature in Figure 5a,b. For CBT, HF gas evolution decreases with increasing concentration of PFPE. In contrast, MBT shows greater HF gas evolution with increasing PFPE concentration. Figure 5c shows the HF gas signal in amp seconds per milligram of PFPE (As/mg) for all samples. The onset of HF gas release is <350 °C, which corresponds to the decomposition of PFPE.[33] The CBT shows a decrease in the release of HF per milligram of PFPE, which indicates either that F bonds are being formed with the other materials in the system or that PFPE decomposition is hindered in some way.

DOI: 10.1021/acsami.5b05238
ACS Appl. Mater. Interfaces 2015, 7, 18742−18749

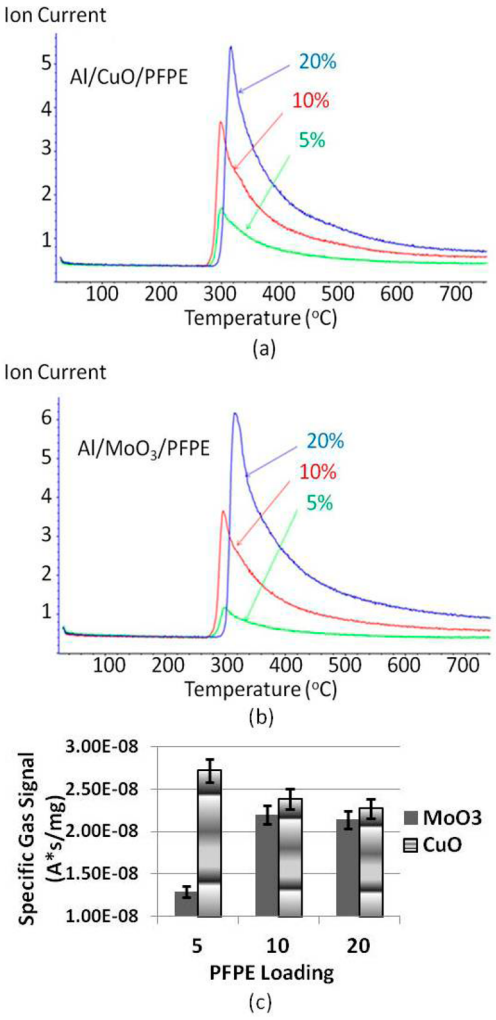

Figure 5. QMS curves for fluorine gas liberated from (a) CBT, (b) MBT, and (c) gas evolution per milligrams of PFPE. The MBT show an increase and limit in HF gas liberation, whereas the CBT show a decrease.

The normalized spectrum for the MBT shows an increase in HF gas produced per milligram of PFPE from 5 to 10%, but there is little change from 10 to 20% PFPE concentration. These data suggest that more Al−F bonds are formed with the MBT than the CBT and are consistent with the magnitudes of the PIR in Figure 4 and Table 2. Specifically, more exothermic PIR is consistent with more Al−F bond formation and lower HF gas evolution.

To identify how F bonds to each component in the combustion products, XPS was performed on products from the MBT and CBT reactions for 5 and 20% PFPE. Figure 6 shows the survey spectrum of the MBT samples (i.e., (a) MBT5, (b) MBT20) and CBT samples (i.e., (c) CBT5 and (d) CBT20). Fluorine bonds are present for all samples. Inspection of these plots shows a comparable signal of every element in the MBT samples but a drastic decline in F signal from CBT5 to CBT20. Upon closer inspection, Mo 3d shows a greater number of pronounced peaks in the MBT5 sample versus MBT20. The peaks at 226 and 229 eV are metallic Mo 3d5/2 and 3d3/2, respectively (see Figure 7).[34] Peaks at 228, 231, 232, and 235 eV are indicative of Mo−O bonds.[34] On the other hand, the CBT show only metallic Cu 2p peaks at 232 and 252 eV for the 3/2 and 1/2 spins, respectively (see Figure 8).[35]

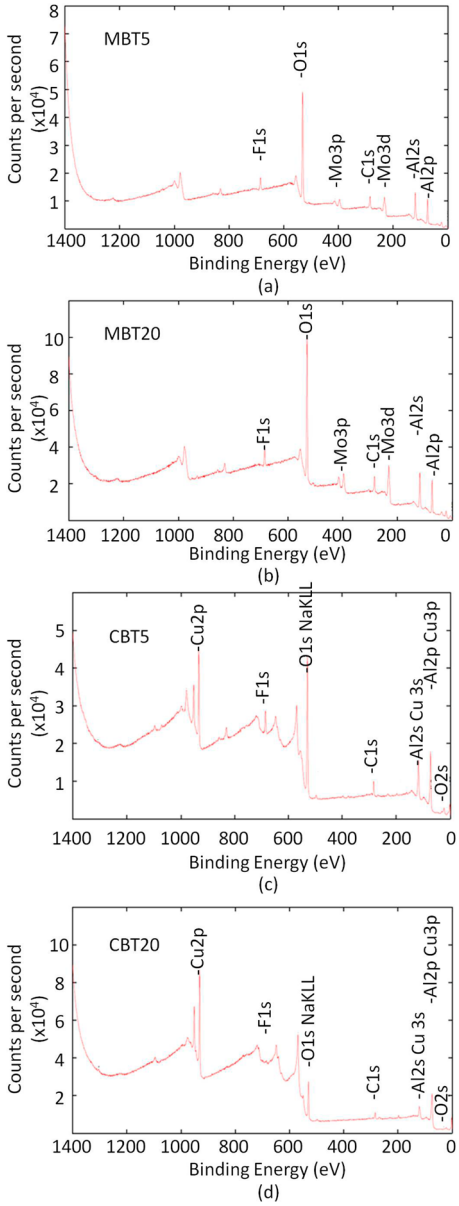

Figure 6. Survey spectra for (a) MBT5, (b) MBT20, (c) CBT5, and (d) CBT20. The relative signal of fluorine decreases significantly from CBT5 to CBT20. (The counts per second axes of the CBT samples are shifted to see the low-intensity peaks in CBT20.)

(There is a small peak at 945 eV in both Cu spectra. This is a Cu 3p3/2 satellite peak.[35]) This also shows that there is no bonding between Cu and F.

Also, due to the presence of the Cu 3s peaks, tight scans of the strong Al 2p peak were not used because they fall in the same binding energy range;[36] instead, Al 2s was analyzed. There is still a Cu 3s peak in the same region, but because there is only one peak from Cu, and the binding energies are spaced well enough to see two distinct peaks, Al 2s was the better candidate for peak identification. For CBT samples, the Al 2s peak comprised Al−O (119 eV) and Al−F (121 eV) binding energies (see Figure 9c,d).[37] It is noted that the peak located at 122 eV in the CBT5 and CBT20 Al spectra is the Cu 3s peak.[35] The Al 2s peak was used for both CBT samples, and Al 2p was used for the MBT samples. The Al 2p line showed Al−O bonds at ∼74.0 eV and Al−F bonds at 75.2 eV (Figure 9a,b). Figure

DOI: 10.1021/acsami.5b05238
ACS Appl. Mater. Interfaces 2015, 7, 18742−18749

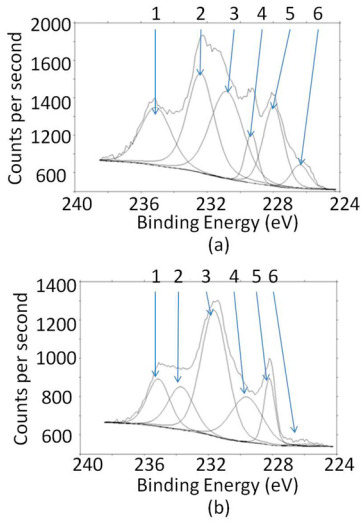

Figure 7. Mo 3d spectral line for (a) MBT5 and (b) MBT20.

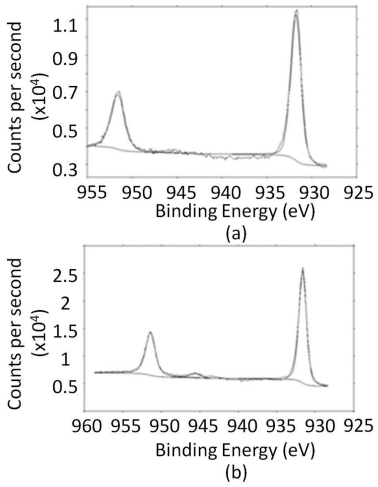

Figure 8. Cu 2p spectral line for (a) CBT5 and (b) CBT20.

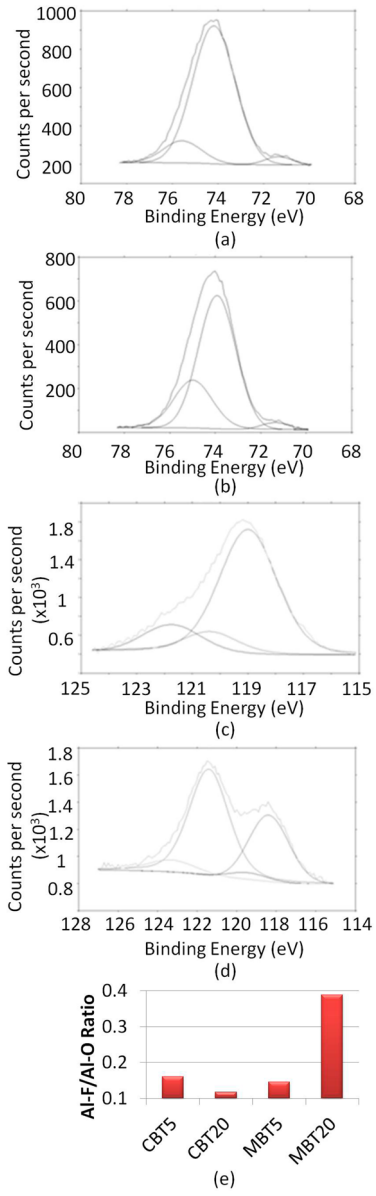

Figure 9. Al 2p spectra for (a) MBT5 and (b) MBT20, Al 2s spectra for (c) CBT5 and (d) CBT20, and (e) graphical representation of Al–F bonds to Al–O bonds present in each sample.

9e shows the ratio of Al–F peak intensity to Al–O peak intensity for each sample. Although Al–F bonds are detected in all samples, the MBT samples show an increase in the ratio of Al–F/Al–O bonding, whereas the CBT samples show a decrease. The increase in Al–F bonding was expected with increasing PFPE loading, but the CBT samples showed a decline. This decline along with the decreasing HF gas signal from CBT5 to CBT20 provides new information about the location of the fluorine.

In addition to Al–F bonds present in CBT samples, the F 1s line shows an additional peak at 688 eV[37] for CBT5 and at 690 eV[38] in the CBT20 sample (see Figure 10c,d). These peaks are both indicative of C–F bonds and were only distinguished in the CBT samples. The MBT samples show only one fluorine peak at 686 eV (Figure 10a,b). This, along with the increase in HF gas production, suggests that the Al–MoO_3 blends catalyze the decomposition of PFPE, whereas the Al–CuO blends do not. This is seen in the F 1s spectra for CBT versus MBT. The improved decomposition of PFPE in the MBT samples along with the increasing formation of Al–F bonds confirms that the low-temperature surface chemistry shown by the PIR increases flame speed in these samples.

CONCLUSION

Combustion characterization analyses using high-speed imaging, XPS, QMS, and DSC were performed for various concentrations of PFPE in Al/MoO_3 and Al/CuO composites to examine the influence of fluorine surface chemistry on reactivity. Results show that the performance of the thermite–PFPE blends is highly dependent on the oxidizing agent. The PFPE blends with MoO_3 show an increase in reactivity, whereas the blends with CuO show a decrease in reactivity when PFPE concentration is increased. We observed a decline in the formation of AlF_3 in CuO-containing samples but an increase in AlF_3 formation in the MoO_3-containing samples. Surface reactions between Al_2O_3 and F from PFPE are less preferred to the thermodynamically favored formation of the Al–O bond from CuO due to its lower bond dissociation energy relative to F or the CF_2 radical. When an oxidizer with a bond dissociation energy similar to that of the C–C or C–F bond (i.e., MoO_3) is

DOI: 10.1021/acsami.5b05238
ACS Appl. Mater. Interfaces 2015, 7, 18742–18749

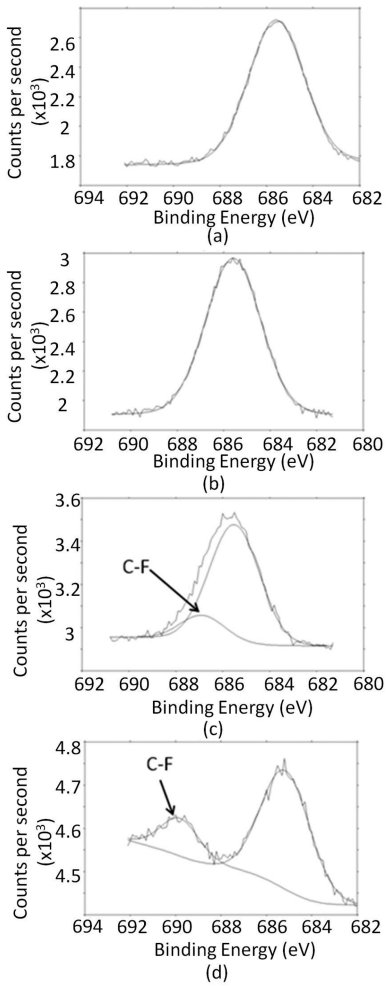

Figure 10. F 1s spectra for (a) MBT5, (b) MBT20, (c) CBT5, and (d) CBT20.

used, PFPE can promote reactivity via catalytic behavior of the Al_2O_3 shell to help decompose PFPE more efficiently and improve the low-temperature surface reactions and overall Al reactivity.

AUTHOR INFORMATION

Corresponding Author

*(M.L.P.) E-mail: michelle.pantoya@ttu.edu.

Notes

The authors declare no competing financial interest.

ACKNOWLEDGMENTS

We are thankful for support from Army Research Office Awards W911NF-11-10439, W911NF-14-10250, and 65092EGRIP and encouragement from our program manager, Dr. Ralph Anthenien. We acknowledge assistance from Drs. Juliusz Warzywoda and Rumesa Tekin in the Materials Characterization Facility in the Whitacre College of Engineering at Texas Tech. We also gratefully acknowledge Dr. Steve Son for the solvent dispersion advice with PFPE.

REFERENCES

(1) Wang, L. L.; Munir, Z. A.; Maximov, Y. M. Thermite Reactions: Their Utilization in the Synthesis and Processing of Materials. *J. Mater. Sci.* **1993**, *28* (14), 3693−3708.

(2) Yen, N. H.; Wang, L. Y. Reactive Metals in Explosives. *Propellants, Explos., Pyrotech.* **2012**, *37* (2), 143−55.

(3) Sullivan, K. T.; Chiou, W.-A.; Fiore, R.; Zachariah, M. R. In Situ Microscopy of Rapidly Heated Nano-Al and Nano-Al/WO_3 Thermites. *Appl. Phys. Lett.* **2010**, *97* (13), 133104.

(4) Pantoya, M.; Granier, J. Combustion Behavior of Highly Energetic Thermites: Nano versus Micron Composites. *Propellants, Explos., Pyrotech.* **2005**, *30* (1), 53−62.

(5) Hunt, E. M.; Pantoya, M. L. Ignition Dynamics and Activation Energies of Metallic Thermites: From Nano- to Micron-Scale Particulate Composites. *J. Appl. Phys.* **2005**, *98* (3), 034909.

(6) Sanders, V. E.; Asay, B. W.; Foley, T. J.; Tappan, B. C.; Pacheco, A. N.; Son, S. F. Reaction Propagation of Four Nanoscale Energetic Composites (Al/MoO_3, Al/WO_3, Al/CuO, and Bi_2O_3). *J. Propul. Power* **2007**, *23* (4), 707−714.

(7) Shigeta, M.; Watanabe, T. Growth Model of Binary Alloy Nanopowders for Thermal Plasma Synthesis. *J. Appl. Phys.* **2010**, *108* (4), 043306.

(8) Deevi, S.; Sikka, V.; Swindeman, C. Application of Reaction Synthesis Principles to Thermal Spray Coatings. *J. Mater. Sci.* **1997**, *32* (12), 3315−3325.

(9) Yeh, C. L.; Huang, Y. S. Thermite Reduction of Ta_2O_5/SiO_2 Powder Mixtures for Combustion Synthesis of Ta-Based Silicides. *J. Alloys Compd.* **2011**, *509* (21), 6302−6306.

(10) Crane, C. a.; Pantoya, M. L.; Dunn, J. Infrared Measurements of Energy Transfer from Energetic Materials to Steel Substrates. *Int. J. Therm. Sci.* **2010**, *49* (10), 1877−1885.

(11) Cervantes, O. G.; Kuntz, J. D.; Gash, A. E.; Munir, Z. A. Activation Energy of Tantalum−Tungsten Oxide Thermite Reactions. *Combust. Flame* **2011**, *158* (1), 117−122.

(12) Iordachescu, M.; Iordachescu, D.; Scutelnicu, E.; Ruiz-Hervias, J.; Valiente, A.; Caballero, L. Influence of Heating Source Position and Dilution Rate in Achieving Overmatched Dissimilar Welded Joints. *Sci. Technol. Weld. Joining* **2010**, *15* (5), 378−385.

(13) Chen, Y.; Lawrence, F. V.; Barkan, C. P. L.; Dantzig, J. A. Heat Transfer Modelling of Rail Thermite Welding. *Proc. Inst. Mech. Eng., Part F* **2006**, *220* (3), 207−217.

(14) Fischer, S.; Grubelich, M. *Theoretical Energy Release of Thermites, Intermetallics, and Combustible Metals*; International Pyrotechnics Seminar, Monterey, CA, USA; Sandia Natinoal Laboratories: Albuquerque, NM, USA, 1998.

(15) Koch, E.-C. *Metal-Fluorocarbon Based Energetic Materials*; Wiley-VCH: Weinheim, Germany, 2012.

(16) Cottrell, T. L. *The Strengths of Chemical Bonds*; Butterworth: London, UK, 1958.

(17) Osborne, D.; Pantoya, M. Effect of Aluminum Particle Size on the Thermal Degradation of Al/Teflon Mixtures. *Combust. Sci. Technol.* **2007**, *179* (8), 1467−1480.

(18) Pantoya, M. L.; Dean, S. W. The Influence of Alumina Passivation on Nano-Al/Teflon Reactions. *Thermochim. Acta* **2009**, *493*, 109−110.

(19) Kappagantula, K. S.; Farley, C.; Pantoya, M. L.; Horn, J. Tuning Energetic Material Reactivity Using Surface Functionalization of Aluminum Fuels. *J. Phys. Chem. C* **2012**, *116* (46), 24469−24475.

(20) Kappagantula, K.; Pantoya, M. L.; Hunt, E. M. Impact Ignition of Aluminum-Teflon Based Energetic Materials Impregnated with Nano-Structured Carbon Additives. *J. Appl. Phys.* **2012**, *112* (2), 024902.

(21) Losada, M.; Chaudhuri, S. Finite Size Effects on aluminum/Teflon Reaction Channels under Combustive Environment: A Rice-Ramsperger-Kassel-Marcus and Transition State Theory Study of Fluorination. *J. Chem. Phys.* **2010**, *133* (13), 134305.

(22) Conner, R. W.; Dlott, D. D. Comparing Boron and Aluminum Nanoparticle Combustion in Teflon Using Ultrafast Emission Spectroscopy. *J. Phys. Chem. C* **2012**, *116* (4), 2751−2760.

(23) Miller, H. a.; Kusel, B. S.; Danielson, S. T.; Neat, J. W.; Avjian, E. K.; Pierson, S. N.; Budy, S. M.; Ball, D. W.; Iacono, S. T.; Kettwich, S. C. Metastable Nanostructured Metallized Fluoropolymer Composites for Energetics. *J. Mater. Chem. A* **2013**, *1* (24), 7050.

DOI: 10.1021/acsami.5b05238
ACS Appl. Mater. Interfaces 2015, 7, 18742−18749

(24) Clayton, N. A.; Kappagantula, K. S.; Pantoya, M. L.; Kettwich, S. C.; Iacono, S. T. Fabrication, Characterization, and Energetic Properties of Metallized Fibers. *Appl. Mater. Interfaces* **2014**, *6*, 6049−6053.
(25) Kettwich, S. C.; Kappagantula, K.; Kusel, B. S.; Avjian, E. K.; Danielson, S. T.; Miller, H. A.; Pantoya, M. L.; Iacono, S. T. Thermal Investigations of Nanoaluminum/Perfluoropolyether Core-Shell Ipregnated Composites for Structural Energetics. *Thermochim. Acta* **2014**, *591*, 45−50.
(26) Jian, G.; Piekiel, N. W.; Zachariah, M. R. Time-Resolved Mass Spectrometry of Nano-Al and Nano-Al/CuO Thermite under Rapid Heating: A Mechanistic Study. *J. Phys. Chem. C* **2012**, *116* (51), 26881−26887.
(27) Wang, H.; Jian, G.; Egan, G. C.; Zachariah, M. R. Assembly and Reactive Properties of Al/CuO Based Nanothermite Microparticles. *Combust. Flame* **2014**, *161* (8), 2203−2208.
(28) Sullivan, K.; Young, G.; Zachariah, M. Enhanced Reactivity of Nano-B/Al/CuO MIC's. *Combust. Flame* **2009**, *156* (2), 302−309.
(29) Moore, D. S.; Son, S. F.; Asay, B. W. Time-Resolved Spectral Emission of Deflagrating Nano-Al and Nano-MoO_3 Metastable Interstitial Composites. *Propellants, Explos., Pyrotech.* **2004**, *29* (2), 106−111.
(30) Cottrell, T. L. *The Strengths of Chemical Bonds*; Butterworth: London, UK, 1958.
(31) Sippel, T. R.; Son, S. F.; Groven, L. J. Altering Reactivity of Aluminum with Selective Inclusion of Polytetrafluoroethylene through Mechanical Activation. *Propellants, Explos., Pyrotech.* **2013**, *38* (2), 286−295.
(32) Puts, G. J.; Crouse, P. L. The Influence of Inorganic Materials on the Pyrolysis of Polytetrafluoroethylene. Part 2: The Common Oxides of Al, Ga, In, Zn, Cu, Ni, Co, Fe, Mn, Cr, V, Zr and La. *J. Fluorine Chem.* **2014**, *168*, 9−15.
(33) Kasai, P. H.; Tang, W. T.; Wheeler, P. Degradation of Perfluoropolyethers Catalyzed by Aluminum Oxide. *Appl. Surf. Sci.* **1991**, *51* (3−4), 201−211.
(34) Al-Kandari, H.; Mohamed, A. M.; Al-Kandari, S.; Al-Kharafi, F.; Mekhemer, G. A.; Zaki, M. I.; Katrib, A. Spectroscopic Characterization−Catalytic Activity Correlation of Molybdena Based Catalysts. *J. Mol. Catal. A: Chem.* **2013**, *368*−*369*, 1−8.
(35) Parmigiani, F.; Pacchioni, G.; Illas, F.; Bagus, P. S. Studies of the Cu□O Bond in Cupric Oxide by X-Ray Photoelectron Spectroscopy and Ab Initio Electronic Structure Models. *J. Electron Spectrosc. Relat. Phenom.* **1992**, *59* (3), 255−269.
(36) Herrera-Fierro, P. Interfacial Chemistry of a Perfluoropolyether Lubricant Studied by X-Ray Photoelectron Spectroscopy and Temperature Desorption Spectroscopy. *J. Vac. Sci. Technol., A* **1993**, *11* (2), 354.
(37) Hess, A.; Kemnitz, E.; Lippitz, A.; Unger, W. E. S.; Menz, D. H. ESCA, XRD, and IR Characterization of Aluminum Oxide, Hydroxyfluoride, and Fluoride Surfaces in Correlation with Their Catalytic Activity in Heterogeneous Halogen Exchange Reactions. *J. Catal.* **1994**, *148*, 270−280.
(38) Lee, J. M.; Kim, S. J.; Kim, J. W.; Kang, P. H.; Nho, Y. C.; Lee, Y. S. A High Resolution XPS Study of Sidewall Functionalized MWCNTs by Fluorination. *J. Ind. Eng. Chem.* **2009**, *15*, 66−71.

DOI: 10.1021/acsami.5b05238
ACS Appl. Mater. Interfaces 2015, 7, 18742−18749